Kinetics of reformation of the S_0 state capable of progressing to the S_1 state after the O_2 release by Photosystem II.

Alain Boussac[a], Julien Sellés[b], Miwa Sugiura[c]

[a] Institut de Biologie Intégrative de la Cellule, UMR 9198, CEA Saclay, 91191 Gif-Sur-Yvette, France. alain.boussac@laposte.net

[b] Institut de Biologie Physico-Chimique, UMR CNRS 7141 and Sorbonne Université, 13 rue Pierre et Marie Curie, 75005 Paris, France. julien.selles@ibpc.fr

[c] Proteo-Science Research Center, Department of Chemistry, Graduate School of Science and Technology, Ehime University, Bunkyo-cho, Matsuyama, Ehime 790-8577, Japan. miwa.sugiura@ehime-u.ac.jp

Corresponding author: Alain Boussac

ORCID numbers:

Alain Boussac: 0000-0002-3441-3861

Miwa Sugiura: 0000-0002-4232-5941

Julien Sellés: 0000-0001-9262-8257

Abbreviations

Photosystem II, PSII; Chl, chlorophyll; Chl_{D1}/Chl_{D2}, monomeric Chl on the D1 or D2 side, respectively; MES, 2-(*N*-morpholino) ethanesulfonic acid; P_{680}, primary electron donor; P_{D1} and P_{D2}, individual Chl on the D1 or D2 side, respectively, which constitute a pair of Chl with partially overlapping aromatic rings; Phe_{D1} and Phe_{D2}, pheophytin on the D1 or D2 side, respectively; PPBQ, phenyl *p*–benzoquinone; Q_A, primary quinone acceptor; Q_B, secondary quinone acceptor; Tyr_Z, the tyrosine 161 of D1 acting as the electron donor to P_{680}; WT*3, *T. elongatus* mutant strain deleted *psbA₁* and *psbA₂* genes and with a His-tag on the carboxy terminus of CP43. DCMU, 3-(3,4-dichlorophényl)-1,1-diméthyl-urée; XFEL, serial femtosecond X-ray free electron laser crystallography.

Key words

Photosystem II, Kok's cycle, S_0 state, Mn_4CaO_5 cluster, Mn_4SrO_5 cluster, Cl^-/Br^- exchange, UV-visible time-resolved absorption changes.

Abstract

The active site for water oxidation in Photosystem II (PSII) comprises a Mn_4CaO_5 cluster adjacent to a redox-active tyrosine residue (Tyr_Z). During the water-splitting process, the enzyme transitions through five sequential oxidation states (S_0 to S_4), with O_2 evolution occurring during the $S_3Tyr_Z^{\bullet}$ to S_0Tyr_Z transition. Chloride also plays a role in this mechanism. Using PSII from *Thermosynechococcus vestitus*, where Ca and Cl were replaced with Sr and Br to slow the $S_3Tyr_Z^{\bullet}$ to $S_0Tyr_Z + O_2$ transition ($t_{1/2}$ ~ 5 ms at room temperature), it was observed that the recovery of a S_0 state, defined as the state able to progress to S_1, exhibits similar kinetics ($t_{1/2}$ ~ 5 ms). This suggests that in CaCl-PSII, the reformation of the functional S_0 state directly follows the $S_3Tyr_Z^{\bullet}$ to $S_0Tyr_Z + O_2$ transition, with no additional delay required for the insertion of a new substrate water molecule (O5) and associated protons.

Introduction

Photosystem II (PSII) in plants, cyanobacteria, and algae by splitting water is at the origin of the atmospheric dioxygen and of the electrons used for making carbohydrates, *e.g.*, [1] for a review. The PSII of *Thermosynechococcus vestitus* (formely *T. elongatus*), the thermophilic cyanobacterium used in this work, consists of 17 trans-membrane proteins and 3 extrinsic membrane proteins [2]. These proteins bind the cofactors involved in the trapping of light and the electron transfer reactions that are: 35 chlorophylls *a* (Chl-*a*), 2 pheophytins (Phe), 1 membrane b-type cytochrome, 1 PSII bound c-type cytochrome (replaced by a 17 kDa protein in plant PSII), 1 non-heme iron, 2 plastoquinones 9 (Q_A and Q_B), the Mn_4CaO_5 cluster, 2 Cl^-, 12 carotenoids and 25 lipids [2].

After the absorption of a photon by one of the 35 chlorophylls of the antenna the excitation energy is transferred to the Chl_{D1}, forming $*Chl_{D1}$. Chl_{D1} belongs to the photochemical trap that consists of the four Chls; P_{D1}, P_{D2}, Chl_{D1}, Chl_{D2}. These 4 Chls, together with the 2 Phe molecules, Phe_{D1} and Phe_{D2}, constitute the reaction center of PSII. A few picoseconds after the formation of the excited $*Chl_{D1}$, a charge separation occurs resulting ultimately in the formation of the $Chl_{D1}^+Phe_{D1}^-$ and then $P_{D1}^+Phe_{D1}^-$ radical pair states, *e.g.* [3-5], and *e.g.* [6,7] for recent theoretical works on this subject. After the charge separation, P_{D1}^+ oxidizes Tyr_Z, the Tyr161 of the D1 polypeptide, and the radical $Tyr_Z^\bullet$ is then reduced by the Mn_4CaO_5 cluster. The electron on Phe_{D1}^- is transferred to Q_A, the primary quinone electron acceptor, and then to Q_B, the second quinone electron acceptor. Whereas Q_A can be only singly reduced under normal conditions, Q_B is doubly reduced and protonated before to leave its site and replaced by an oxidized Q_B from the membrane pool, *e.g.* [8-11] and references therein.

The Mn_4CaO_5 cluster cycles through five redox states denoted S_n, where n stands for the number of stored oxidizing equivalents. The S_1-state is stable in the dark and therefore S_1 is the preponderant state upon dark adaptation. When the S_4-state is formed after the 3rd flash of light given on dark-adapted PSII, two water molecules bound to the cluster are oxidized, O_2 is released and the S_0-state is reformed [12,13].

Thanks to the advent of serial femtosecond X-ray free electron laser crystallography (XFEL), the structure of the Mn_4CaO_5 cluster have been resolved in the dark-adapted state with the 4 Mn ions in a redox state as close as possible to that in the S_1-state, *i.e.* $Mn^{III}_2Mn^{IV}_2$ [2,14-

20]. The Mn_4CaO_5 structure resemble a distorted chair including a μ-oxo-bridged cuboidal Mn_3O_4Ca unit with a fourth Mn attached to this core structure *via* two μ-oxo bridges involving the two oxygen's O_4 and O_5. Important progresses have been recently done in the resolution of the crystal structures in the S_2 and S_3 states [14-20]. The structural changes identified in the S_1 to S_2 transition, and those more numerous in the S_2 to S_3 transition cannot be detailed in a few lines. Very briefly, these works show that, when compared to S_1, the changes in S_2 are minor and more or less correspond to those expected for the valence change of the dangler Mn4 from +III to +IV, *e.g.*, [21]. Importantly, water molecules in the "O1" and "O4" channels, defined as such because they start from the O1 and O4 oxygens of the cluster, appeared localized slightly differently in S_2 than in S_1 [17,20]. In contrast, in the S_2 to S_3 transition, major structural changes have been detected together with the insertion of a 6th oxygen, originally a water molecule close to Ca and labelled O6 or Ox, finally bridging Mn1 and Ca [15,18-20]. The insertion of this 6th oxygen was shown to be complete in 400 μs, and to occur simultaneously with the oxidation of Mn1 from +III to +IV [19,20]. This newly bound oxygen on Mn1 is supposed to correspond to the second water substrate molecule and is at a short distance of the bridging oxygen O5 supposed to be the first, and slowly exchangeable, bound water substrate molecule, *e.g.*, [15,16,18,20,22]. An important movement of the Glu189 residue would allow its carboxylate chain to make a hydrogen bond with the protonated form of this 6th oxygen in S_3 [17,20].

There is a model, increasingly shared, in which after the 3rd flash O_2 is formed by a reaction between O5 and O6, even if the details including the way used by the released protons, are still being debated, *e.g.*, [19,20,22-29].

Reformation of the S_0 state after O_2 evolution is less studied. This is partly explained by the fact that after each flash at least 10% of the PSII do not progress to the next S_n state. This implies that after 3 flashes the mix of the S_n states, *e.g.*, [30], strongly complicates the interpretation of the data. The "S_4" to S_0 transition corresponds to the reduction of the Mn ions of the cluster, to the insertion to one of the two water substrate molecules and to some reprotonations [23,31]. Two to four ms after the 3rd flash, the structure solved by XFEL of the Mn_4CaO_5 cluster and around, appeared to be the final one. Therefore, the S_0 state appears to be reformed in all the centers in 4 ms [19], a time corresponding to the release of O_2 in 100% of the centers [32,33]. It is however questionable whether this S_0 state is fully functional and capable of being oxidized to S_1, see [31,34] for recent computational works on this issue. Here, for an

experimental kinetic approach, the advancement of the S_n state cycle was followed by measuring the ΔI/I induced at 292 nm by each flash of a sequence [33,35], and in which an (additional) extra saturating flash was given at varied time (Δt) after the third one, *e.g.* [36]. For the too short Δt values, the centers are expected to be unable to progress to the next S_n state, and the flash following this Δt should have no effect on the period 4 oscillation. When the Δt increases, a shift in oscillations is expected, as the additional flash has more and more the effect of a fourth flash, which gives the kinetics for the reformation of a functional S_0 state.

Materials and Methods

Culture of *T. vestitus* WT3* cells in the presence of Sr^{2+} and Br^-, instead of Ca^{2+} and Cl^-, was done as previously described [33]. Purification of the SrBr-PSII was done with the same protocol described in [37].

Time-resolved absorption changes measurements were performed with a lab-built spectrophotometer [38] slightly modified as detailed in [37]. Absorption changes were sampled at discrete times after the actinic flash by short weak measuring flashes. These measuring flashes were provided by an optical parametric oscillator (Horizon OPO, Amplitude Technologies) pumped by a frequency tripled Nd:YAG laser (Surelite II, Amplitude Technologies), producing monochromatic flashes (355 nm, 2 nm full-width at half-maximum) with a duration of 5 ns. Actinic flashes, for all the samples studied, were provided by a second Nd:YAG laser (Surelite II, Amplitude Technologies) at 532 nm, which pumped an optical parametric oscillator (Surelite OPO plus) producing monochromatic saturating flashes at 695 nm with the same pulse-length. The time delay between the laser delivering the actinic flashes and the laser delivering the detector flashes was controlled by a digital delay/pulse generator (DG645, jitter of 1 ps, Stanford Research). The path-length of the cuvette was 2.5 mm. The analytical flash was split into two parts using an optical guide composed by a bunch of randomized optical fibers. One part is connected to the reference cuvette for the measurement of the I_0 and the other part is connected to the second cuvette, for the measurement of I, and to which is also connected the optic fiber from the actinic flash. The ΔI/I is equivalent to the $(I-I_0)/I$ value.

In this work, the absorption changes have been measured at 292 nm. This wavelength corresponds to an isosbestic point for Q_A^-/Q_A, and $PPBQ^-/PPBQH_2$, the added electron acceptor,

and is in a spectral region where the absorption of the Mn_4CaO_5 cluster depends on the S_n-states which allow us to detect oscillations with a period four [35].

Once purified, the Ca and Sr do not exchange in the PSII [33] in contrast to the chloride, which can be replaced by bromide or iodide [39]. Therefore, for the ΔI/I measurements the samples were diluted in 1 M betaine, 15 mM $CaBr_2$, 15 mM $MgBr_2$, and 40 mM MES (pH 6.5). PSII samples were then dark-adapted for ~ 1 h at room temperature (20–22 °C) before the addition of 0.1 mM phenyl *p*–benzoquinone (PPBQ) dissolved in dimethyl sulfoxide. The chlorophyll concentration of all the samples was ~ 25 μg of Chl mL^{-1}.

Results and discussion

The constraint for measuring the "reopening" of the electron donor side of PSII after the 3rd actinic flash given to dark-adapted PSII is that the kinetics for the reoxidation of Q_A^- must be faster than the $S_3Tyr_Z^\bullet$ to S_0 +O_2 step. Since the electron transfer from Q_A^- to Q_B occurs with a $t_{1/2}$ value between 500 μs and ~ 1-2 ms, *e.g.* [40], these conditions can only be fulfilled in PSII in which the Ca and Cl have been replaced by Sr and Br [33], and in which the $t_{1/2}$ for the $S_3Tyr_Z^\bullet$ to S_0 +O_2 step was slowed down to ~ 5-7 ms.

Fig. 1 shows a control experiment in which the amplitude of absorption changes induced by each saturating flash, at 695 nm, of a series (200 ms apart) in the SrBr-PSII (with PPBQ present) used in this work was measured. The ΔI/I were measured by using a weak measuring flash at 292 nm, given 100 ms after each flash of the sequence. The oscillating pattern with a period of four [35] is similar to that already reported, and described in detail, in the SrBr-PSII [33].

Fig. 2 shows the absorption changes, at 292 nm, from 10 μs (*i.e.* in the $S_nTyr_Z^\bullet$ state) to the ms time range (*i.e.* in the $S_{n+1}Tyr_Z$ state) after the first 3 flashes given to a dark-adapted SrBr-PSII. This experiment allows us to assess the kinetics of the S-state transition after the first flash (black), the second flash (red) and the third flash (blue). At 292 nm, the absorption changes associated with the $S_2Tyr_Z^\bullet \rightarrow S_3Tyr_Z$ transition on the second flash (red trace) are small and preclude a reliable kinetic analysis. As already observed [33], the kinetics of the absorption changes in the $S_1Tyr_Z^\bullet \rightarrow S_2Tyr_Z$ (black trace) with a $t_{1/2}$ ~ 200 μs is slightly slower in SrBr-PSII than in CaCl-PSII in which the $t_{1/2}$ is ~ 50 μs. In the $S_3Tyr_Z^\bullet$ to S_0Tyr_Z transition (blue trace), two

phases are observed [32,41,42]. The fast phase with a $t_{1/2}$ ~ 50 to 100 µs in *T. vestitus* [33], which corresponds to the release of the first proton in this transition before the reduction of $Tyr_Z^{\bullet}$ by the Mn cluster, is seen as a lag phase at 292 nm [43]. The slow phase, seen here as an absorption decay with a $t_{1/2}$ ~ 5 ms corresponds to the S_0 and O_2 formations and to the release of an additional proton, *e.g.*, [43,44].

To ensure that the kinetics for the oxidation of Q_A^- is indeed significantly faster than the $S_3Tyr_Z^{\bullet}$ to S_0Tyr_Z transition, an experiment was carried out to estimate the reoxidation of Q_A^- in the SrBr-PSII used here. Panel A in Fig. 3 shows the protocol used. It is based on the approach in [36]. In this experiment, the ΔI/I were recorded 100 ms after each flash of a sequence (green arrows) alternately without and with an extra saturating flash (red arrow) given Δt after the first flash. The sequence without the extra flash provides as many ΔI/I values corresponding to the first flash as sequences with the extra flash after the first flash, thus avoiding using the same data corresponding to the first flash for all Δt values.

Panel B in Fig. 3 shows the flash dependent ΔI/I values for Δt values ranging from 10 µs to several ms (the color code for the Δt in µs is on the right part of the Panel). When the extra flash was given 10 µs after the first flash the centers were still closed with both $Tyr_Z^{\bullet}$ and Q_A^- being largely present. Consequently for ΔT = 10 µs, the ΔI/I after the 3rd flash is close to that after the 3rd flash in Fig. 1 since the extra flash has no effect. For longer Δt values between the first flash and the extra flash in red in Panel A of Fig. 3 the reaction centers become more and more "reopen". The reopening occurs firstly on the donor side and then, in a second phase, on the acceptor side, so that the flash labelled "2nd" flash on the X-axis of panel B in Fig. 3 corresponds actually to a 3rd flash as defined in Fig. 1. The kinetics of the reopening of the centers after the first flash was estimated by plotting the ΔI/I measured after the 3rd flash *minus* the ΔI/I measured after the 2nd flash. Panel C in Fig. 3 shows this plot. Despite the limited number of data points, we can hypothesize that the decay observed in the 100 to 200 µs time range corresponds well to the $S_1Tyr_Z^{\bullet} \rightarrow S_2Tyr_Z$ kinetics. For its part, the slow phase with a $t_{1/2}$ ~ 1 ms fit well with the reoxidation of Q_A^- [40,45]. Two comments can be made here: *i*) the fast phase is detected probably in centers in which Q_A^- is oxidized by the non-heme iron with a kinetics much faster than the $S_1Tyr_Z^{\bullet} \rightarrow S_2Tyr_Z$ kinetics, and *ii*) the reoxidation of Q_A^- ($t_{1/2}$ ~ 1 ms, [40,45]) occurs more rapidly than the $S_3Tyr_Z^{\bullet}$ to S_0Tyr_Z transition ($t_{1/2}$ ~ 5 ms), [33] and Fig. 2. The $t_{1/2}$ for the reoxidation of Q_A^- by the oxidized non-heme iron has been estimated to be ~ 55 µs [10]. This

kinetics has been measured with DCMU bound, a condition known to increase the E_m of Q_A by ~ 50 mV [46,47] and therefore to likely slow down the electron transfer from Q_A^- to Fe^{3+}. That means that the value of 55 µs is probably an upper limit in the absence of DCMU.

The conditions are now established for measuring the kinetics at which a functional S_0 state is formed after 3 flashes and after O_2 is evolved. Panel A in Fig. 4 shows the protocol used for that. In this experiment, the ΔI/I were also recorded 100 ms after each flash of a sequence (green arrows) alternately without and with an extra flash (red arrow) given Δt after the third flash. The sequence without the extra flash drawn in red in Panel A, provides as many ΔI/I values corresponding to the first 3 flashes as sequences with the extra flash, thus avoiding using the same data corresponding to these first 3 flashes for all Δt values.

Panel B in Fig. 4 shows the flash dependent ΔI/I values with Δt values ranging from 10 µs to several ms between the 3rd flash and the extra flash (the color code for the Δt in µs is on the right part of the Panel). As for the experiment reported in Fig. 3, when the Δt was 10 µs, both $Tyr_Z^\bullet$ and Q_A^- remains largely present, so that the ΔI/I after the 4th actinic flash is close to that after the 4th actinic flash in Fig. 1. For longer Δt values the flash labelled "4th" flash on the X-axis of panel B in Fig. 4 has a ΔI/I value close to that after the 5th flash as defined on the X-axis of Fig. 1.

The black data points in Panel C of Fig. 4 shows the amplitude of the ΔI/I measured after the fourth flash *minus* the ΔI/I measured after the third flash (normalized to 100% for Δt = 100 ms). We can apply here the same reasoning as for the experiment reported in Fig. 3. For the shortest Δt values, *e.g.*, 10 µs between the 3rd actinic flash and the extra flash drawn in red in Panel A, the centers are still in the $S_3Tyr_Z^\bullet$ state before the process resulting in the O_2 formation and the before the release of protons begins. In other terms, it has no effect because the centers are closed. When the Δt increases, the proportion of S_0 increases as the centers reopen. The red data points are a replot of the $S_3Tyr_Z^\bullet$ to S_0Tyr_Z transition at 292 nm shown in Fig. 2 (after a normalization of the data from 100 % for the ΔI/I at t = 10 µs to 0 % for the ΔI/I at t = 100 ms). The resemblance between the 2 kinetics is remarkable. This resemblance shows that the kinetics of the formation of a S_0-state capable of progressing to S_1 follows the kinetics of O_2 evolution without any apparent lag.

Conclusion

After the third flash, the Mn_4 cluster in the S_n state, called here S_0, capable to progress to S_1 with the same kinetics as the $S_3Tyr_Z^{\bullet}$ to $S_0Tyr_Z + O_2$ transition. This means than the rebinding of the water molecule to the cluster, *i.e.*, the rebinding of O5, and all the proton bindings and movements [23,31,34] have a kinetics equal or faster than the regeneration of an S_0 state capable of progressing to S_1 after a fourth flash. This kinetics has been measured in SrBr-PSII in order the Q_A^- reoxidation kinetics was not limiting. This imply that the kinetics of the recovery of a functional S_0 corresponds to the situation in SrBr-PSII and the $t_{1/2}$ ~ 5 ms can only be considered as upper limit in CaCl-PSII. Our data do not allow us to kinetically identify all the intermediate states seen in the $S_3Tyr_Z^{\bullet}$ to $S_0Tyr_Z + O_2$, *e.g.*, [19,48], however, from the strong similarity between the recovery of a functional S_0 state and the $S_3Tyr_Z^{\bullet}$ to $S_0Tyr_Z + O_2$ transition in Panel C of Fig. 4, it sems likely that the reformation of a functional S_0 state also follows the $S_3Tyr_Z^{\bullet}$ to $S_0Tyr_Z + O_2$ transition in CaCl-PSII.

Acknowledgements

This study was supported by i) the JSPS-KAKENHI Grant 21H02447 (MS), (ii) the Labex Dynamo ANR-11-LABX-0011-01 (JS).

Legend of figures

Figure 1: Sequence of the amplitude of the absorption changes at 292 nm. Measurements were done during a series of saturating flashes (spaced 200 ms apart) given on SrBr-PSII. The sample (Chl = 25 µg mL^{-1}) was dark-adapted for 1 h at room temperature before the addition of 100 µM PPBQ (dissolved in dimethyl-sulfoxide). The term "flash number" refers to the number of actinic flashes applied to the dark-adapted sample. The signal (ΔI/I on the Y-axis) was measured using a weak flash at 292 nm, 100 ms after each actinic flash. The continuous line is drawn for joining the data points.

Figure 2: Kinetics of the absorption changes at 292 nm after the first flash (black points), the second flash (red points), and the third flash (blue points), given to dark-adapted SrBr-PSII. Other experimental conditions were similar to those in Fig. 1.

Figure 3: Panel A, schematic view of the protocol used. An extra actinic flash was given Δt after the 1st actinic flash; Panel B, oscillations of the ΔI/I after each flash of a sequence *versus* the Δt between the first flash and the extra flash to SrBr-PSII; Panel C, Amplitude of the ΔI/I measured after the third flash *minus* the ΔI/I measured after the second flash (normalized to 100 % for Δt = 10 µs and to 0 % for Δt = 100 ms). Other experimental conditions were similar to those in Fig. 1.

Figure 4: Panel A, schematic view of the protocol used when the extra actinic flash was given after the third actinic flash; Panel B, oscillations of the ΔI/I after each flash of the sequence *versus* the Δt between the third flash and the extra flash to SrBr-PSII; Panel C; The black points are the amplitude of the ΔI/I measured after the fourth flash *minus* the ΔI/I measured after the third flash (in Panel B, and the red data points are the ΔI/I after the third flash and shown in Fig. 2 The values are normalized to 100 % for Δt = 10 µs and to 0 % for Δt = 100 ms. Other experimental conditions were similar to those in Fig. 1.

References

[1] Shevela D, Kern JF, Govindjee G, Messinger J (2023) Solar energy conversion by photosystem II: principles and structures. Photosynth Res 156:279–307. https://doi.org/10.1007/s11120-022-00991-y

[2] Suga M, Akita F, Hirata K, Ueno G, Murakami H, Nakajima Y, Shimizu T, Yamashita K, Yamamoto M, Ago H, Shen J-R (2015) Native structure of photosystem II at 1.95 angstrom resolution viewed by femtosecond X-ray pulses. Nature 517:99–103. https://doi.org/10.1038/nature13991

[3] Holzwarth AR, Müller MG, Reus M, Nowaczyk M, Sander J, Rögner M (2006) Kinetics and mechanism of electron transfer in intact photosystem II and in the isolated reaction center: pheophytin is the primary electron acceptor. Proc Natl Acad Sci USA 103:6895–6900. https://doi.org/10.1073/pnas.0505371103

[4] Romero E, Novoderezhkin VI, van Grondelle R (2017) Quantum design of photosynthesis for bio-inspired solar-energy conversion. Nature 543: 355–365. https://doi.org/10.1038/nature22012

[5] Diner BA, Schlodder E, Nixon PJ, Coleman WJ, Rappaport F, Lavergne J, Vermaas WFJ, Chisholm DA (2001) Site-directed mutations at D1-His198 and D2-His197 of photosystem II in *Synechocystis* PCC 6803: sites of primary charge separation and cation and triplet stabilization. Biochemistry 24:9265–9281. https://doi.org/10.1021/bi010121r

[6] Müh F, Plöckinger M, Renger T (2017) Electrostatic asymmetry in the reaction center of photosystem II. J Phys Chem Lett 8:850–858. https://doi.org/10.1021/acs.jpclett.6b02823

[7] Sirohiwal A, Pantazis DA (2023) Reaction center excitation in Photosystem II: From multiscale modeling to functional principles. Acc Chem Res 56:2921–2932. https://doi.org/10.1021/acs.accounts.3c00392

[8] Fufezan C, Zhang C-X, Krieger-Liszkay A, Rutherford AW (2005) Secondary quinone in photosystem II of *Thermosynechococcus elongatus*: semiquinone-iron EPR signals and

temperature dependence of electron transfer. Biochemistry 44:12780–12789. https://doi.org/10.1021/bi051000k

[9] Sedoud A, Cox N, Sugiura M, Lubitz W, Boussac A, Rutherford AW (2011) The semiquinone-iron complex of photosystem II: EPR signals assigned to the low field edge of the ground state doublet of $Q_A^{\bullet-}Fe^{2+}$ and $Q_B^{\bullet-}Fe^{2+}$. Biochemistry 50:6012–6021. https://doi.org/10.1021/bi200313p

[10] Boussac A, Sugiura M, Rappaport F (2010) Probing the quinone binding site of photosystem II from *Thermosynechococcus elongatus* containing either PsbA1 or PsbA3 as the D1 protein through the binding characteristics of herbicides. Biochim Biophys Acta 1807:119–129. https://doi.org/10.1016/j.bbabio.2010.10.004

[11] de Causmaecker S, Douglass JS, Fantuzzi A, Nitschke W, Rutherford AW (2019) Energetics of the exchangeable quinone, Q_B, in Photosystem II. Proc Natl Acad Sci USA 116:19458–19463. https://doi.org/10.1073/pnas.1910675116

[12] Joliot P, Barbieri G, Chabaud R (1969) A new model of photochemical centers in system 2. Photochem Photobiol 10:309–329. https://doi.org/10.1111/j.1751-1097.1969.tb05696.x

[13] Kok B, Forbush B, McGloin M (1970) Cooperation of charges in photosynthetic O_2 evolution–I. A linear four step mechanism. Photochem Photobiol 11:457–475. https://doi.org/10.1111/j.1751-1097.1970.tb06017.x

[14] Young ID, Ibrahim M, Chatterjee R, Gul S, Fuller FD, Koroidov S, Brewster AS, Tran R, Alonso-Mori R, Kroll T, Michels-Clark T, Laksmono H, Sierra RG, Stan CA, Hussein R, Zhang M, Douthit L, Kubin M, de Lichtenberg C, Pham LV, Nilsson H, Cheah MH, Shevela D, Saracini C, Bean MA, Seuffert I, Sokaras D, Weng T-C, Pastor E, Weninger C, Fransson T, Lassalle L, Bräuer P, Aller P, Docker PT, Andi B, Orville AM, Glownia JM, Nelson S, Sikorski M, Zhu D, Hunter MS, Lane TJ, Aquila A, Koglin JE, Robinson J, Liang M, Boutet S, Lyubimov AY, Uervirojnangkoorn M, Moriarty NW, Liebschner D, Afonine PV, Waterman DG, Evans G, Wernet P, Dobbek H, Weis WI, Brunger AT, Zwart PH, Adams PD, Zouni A, Messinger J, Bergmann U, Sauter NK, Kern J, Yachandra VK, Yano J (2013) Structure of photosystem II and substrate binding at room temperature. Nature 540:453–474. https://doi.org/10.1038/nature20161

[15] Ibrahim M, Fransson T, Chatterjee R, Cheah MH, Hussein R, Lassalle L, Sutherlin KD, Young ID, Fuller FD, Gul S, Kim IS, Simon PS, de Lichtenberg C, Chernev P, Bogacz I, Pham CC, Orville AM, Saichek N, Northen T, Batyuk A, Carbajo S, Alonso-Mori R, Tono K, Owada S, Bhowmick A, Bolotovsky R, Mendez D, Moriarty NW, Holton JM, Dobbek H, Brewster AS, Adams PD, Sauter NK, Bergmann U, Zouni A, Messinger J, Kern J, Yachandra VK, Yano J (2020) Untangling the sequence of events during the $S_2 \rightarrow S_3$ transition in photosystem II and implications for the water oxidation mechanism. Proc Natl Acad Sci USA 117:12624–12635. https://doi.org/10.1073/pnas.2000529117.

[16] Hussein R, Ibrahim M, Bhowmick A, Simon PS, Chatterjee R, Lassalle L, Doyle M, Bogacz I, Kim I-S, Cheah MH, Gul S, de Lichtenberg C, Chernev P, Pham CC, Young ID, Carbajo S, Fuller FD, Alonso-Mori R, Batyuk A, Sutherlin KS, Brewster AS, Bolotovsky R, Mendez D, Holton JM, Moriarty NW, Adams PD, Bergmann U, Sauter NK, Dobbek H, Messinger J, Zouni A, Kern J, Yachandra VK, Yano J (2021) Structural dynamics in the water and proton channels of photosystem II during the S_2 to S_3 transition. Nat Commun 12:6531. https://doi.org/10.1038/s41467-021-26781-z

[17] Li HJ, Nakajima Y, Nomura T, Sugahara M, Yonekura S, Chan SK, Nakane T, Yamane T, Umena Y, Suzuki M, Masuda T, Motomura T, Naitow H, Matsuura Y, Kimura T, Tono K, Owada S, Joti Y, Tanaka R, Nango E, Akita F, Kubo M, Iwata S, Shen J-R, Suga M (2021) Capturing structural changes of the S_1 to S_2 transition of photosystem II using time-resolved serial femtosecond crystallography. IUCrJ 8:431–443. https://doi.org/10.1107/S2052252521002177 .

[18] Suga M, Akita F, Yamashita K, Nakajima Y, Ueno G, Li HG, Yamane T, Hirata K, Umena Y, Yonekura S, Yu LJ, Murakami H, Nomura T, Kimura T, Kubo M, Baba S, Kumasaka T, Tono K, Yabashi M, Isobe H, Yamaguchi K, Yamamoto M, Ago H, Shen J-R (2019) An oxyl/oxo mechanism for oxygen-oxygen coupling in PSII revealed by an x-ray free-electron laser. Science 366:334–338. https://doi.org/10.1126/science.aax6998 .

[19] Bhowmick A, Simon PS, Bogacz I, Hussein R, Zhang M, Makita H, Ibrahim M, Chatterjee R, Doyle MD, Hon Cheah M, Chernev P, Fuller FD, Fransson T, Alonso-Mori R, Brewster AS, Sauter NK, Bergmann U, Dobbek H, Zouni A, Messinger J, Kern J, Yachandra VK, Yano J

(2023) Going around the Kok cycle of the water oxidation reaction with femtosecond X-ray crystallography. IUCrJ 10:642–655. https://doi.org/10.1107/S2052252523008928

[20] Li H, Nakajima Y, Nango E, Owada S, Yamada D, Hashimoto K, Luo F, Tanaka R, Akita F, Kato K, Kang J, Saitoh Y, Kishi S, Yu H, Matsubara N, Fujii H, Sugahara M, Suzuki M, Masuda T, Kimura T, Thao TN, Yonekura S, Yu L-J, Tosha T, Tono K, Joti Y, Hatsui T, Yabashi M, Kubo M, Iwata S, Isobe H, Yamaguchi K, Suga M, Shen J-R (2024) Oxygen-evolving photosystem II structures during S_1–S_2–S_3 transitions. Nature 626:670–677. https://doi.org/10.1038/s41586-023-06987-5

[21] Krewald V, Neese F, Pantazis DA (2015) Resolving the manganese oxidation states in the oxygen-evolving catalyst of natural photosynthesis. Isr J Chem 55:1219–1232. https://doi.org/10.1002/ijch.201500051

[22] de Lichtenberg C, Rapatskiy L, Reus M, Heyno E, Schnegg A, Nowaczyk MM, Lubitz W, Messinger J, Cox N (2024) Assignment of the slowly exchanging substrate water of nature's water-splitting cofactor. Proc Natl Acad Sci USA 121:2319374121. https://doi.org/10.1073/pnas.2319374121

[23] Siegbahn PEM (2013) Water oxidation mechanism in photosystem II, including oxidations, proton release pathways, O—O bond formation and O_2 release. Biochim Biophys Acta 1827:1003–1019. http://dx.doi.org/10.1016/j.bbabio.2012.10.006

[24] Siegbahn PEM (2017) Nucleophilic water attack is not a possible mechanism for O-O bond formation in photosystem II. Proc Natl Acad Sci USA 114:4966–4968. https://doi.org/10.1073/pnas.1617843114

[25] Siegbahn PEM (2017) Computational investigations of S_3 structures related to a recent X-ray free electron laser study. Chem Phys Lett 690:172–176. https://doi.org/10.1016/j.cplett.2017.08.050

[26] Malcomson T, Rummel F, Barchenko M, O'Malley P (2024) Hey ho, where'd the proton go? Final deprotonation of O6 within the S_3 state of photosystem II. J Photochem Photobiol B: Biol 257:112946. https://doi.org/10.1016/j.jphotobiol.2024.112946

[27] Allgöwer F, Pöverlein MC, Rutherford AW, Kaila VRI (2024) Mechanism of proton release during water oxidation in Photosystem II. BiorXiv, https://doi.org/10.1101/2024.07.03.602004

[28] Noguchi T (2024) Mechanism of proton transfer through the D1-E65/D2-E312 gate during photosynthetic water oxidation. J Phys Chem B 128:1866–1875. https://doi.org/10.1021/acs.jpcb.3c07787

[29] Drosou M, Pantazis DA (2021) Redox isomerism in the S_3 state of the oxygen-evolving complex resolved by coupled cluster theory. Chem Eur J 27:12815–12825. https://doi.org/10.1002/chem.202101567

[30] Han G, Chernev P, Styring S, Messinger J, Mamedov F (2022) Molecular basis for turnover inefficiencies (misses) during water oxidation in photosystem II. Chem Sci 13:8667–8678. https://doi.org/10.1039/d2sc00854h

[31] Guo Y, He L, Ding Y, Kloo L, Pantazis DA, Messinger J, Sun L (2024) Closing Kok's cycle of nature's water oxidation catalysis. Nat Commun 15:5982. https://doi.org/10.1038/s41467-024-50210-6

[32] Rappaport F, Blanchard-Desce M, Lavergne J (1994) Kinetics of electron-transfer and electrochromic change during the redox transitions of the photosynthetic oxygen evolving complex. Biochim Biophys Acta 1184:178–192. https://doi.org/10.1016/0005-2728(94)90222-4

[33] Ishida N, Sugiura M, Rappaport F, Lai TL, Rutherford AW, Boussac A (2008) Biosynthetic exchange of bromide for chloride and strontium for calcium in the photosystem II oxygen-evolving enzymes. J Biol Chem 283:13330–13340. https://doi.org/10.1074/jbc.M710583200

[34] Capone M, Narzi D, Guidoni L (2021) Mechanism of oxygen evolution and Mn_4CaO_5 cluster restoration in the natural water-oxidizing catalyst. Biochemistry 60:2341–2348. https://doi.org/10.1021/acs.biochem.1c00226

[35] Lavergne J (1991) Improved UV-visible spectra of the S-transitions in the photosynthetic oxygen-evolving system. Biochim Biophys Acta 1060:175–188. https://doi.org/10.1016/S0005-2728(09)91005-2

[36] Bouges-Bocquet B (1973) Limiting steps in Photosystem II and water decomposition in *Chlorella* and spinach chloroplasts. Biochim Biophys Acta 292:772–785. https://doi.org/10.1016/0005-2728(73)90024-8

[37] Sugiura M, Taniguchi T, Tango N, Nakamura M, Sellés J, Boussac A (2021) Probing the role of arginine 323 of the D1 protein in photosystem II function. Physiol Plant 171:183–199. https://doi.org/10.1111/ppl.13115

[38] Béal D, Rappaport F, Joliot P (1999) A new high-sensitivity 10-ns time-resolution spectrophotometric technique adapted to in vivo analysis of the photosynthetic apparatus. Rev Sci Instrum 70:202–207. https://doi.org/10.1063/1.1149566

[39] Boussac A, Ishida N, Sugiura M, Rappaport F (2012) Probing the role of chloride in Photosystem II from *Thermosynechococcus elongatus* by exchanging chloride for iodide. Biochim Biophys Acta 1817:802–810. https://doi.org/10.1016/j.bbabio.2012.02.031

[40] Boussac A, Sellés J, Hamon M, Sugiura M (2022) Properties of Photosystem II lacking the PsbJ subunit. Photosynth Res 152:347–361. https://doi.org/10.1007/s11120-021-00880-w

[41] Koike H, Hanssum B, Inoue Y, Renger G (1987) Temperature dependence of S-state transition in a thermophilic cyanobacterium, *Synechococcus vulcanus* Copeland measured by absorption changes in the ultraviolet region. Biochim Biophys Acta 893:524–533. https://doi.org/10.1016/0005-2728(87)90104-6

[42] Haumann M, Liebisch P, Muller C, Barra M, Grabolle M, Dau H (2005) Photosynthetic O_2 formation tracked by time-resolved X-ray experiments. Science 310:1019–1021. https://doi.org/10.1126/science.1117551

[43] Rappaport F, Lavergne J (1991) Proton release during successive oxidation steps of the photosynthetic water oxidation process - stoichiometries and pH-dependence. Biochemistry 30:10004–10012. https://doi.org/10.1021/bi00105a027

[44] Boussac A, Sugiura M, Sellés J (2022) Probing the proton release by Photosystem II in the S_1 to S_2 high-spin transition. Biochim Biophys Acta 1863:148546. https://doi.org/10.1016/j.bbabio.2022.148546

[45] de Wijn R, van Gorkom HJ (2001) Kinetics of electron transfer from Q_A to Q_B in Photosystem II. Biochemistry 40:11912–11922. https://doi.org/10.1021/bi010852r

[46] Krieger-Liszkay A, Rutherford AW (1998) Influence of herbicide binding on the redox potential of the quinone acceptor in photosystem-II. Relevance to photodamage and phytotoxicity. Biochemistry 37:17339–17344. https://doi.org/10.1021/bi9822628

[47] Krieger-Liszkay A, Rutherford AW (2001) Herbicide-induced oxidative stress in Photosystem II. Trends Biochem Sci 26:648–653. https://doi.org/10.1016/S0968-0004(01)01953-3

[48] Greife P. Schönborn M, Capone M, Assunçao R, Narzi D, Guidoni L, Dau H (2023) The electron-proton bottleneck of photosynthetic oxygen evolution. Nature 617: 623–628. https://doi.org/10.1038/s41586-023-06008-5

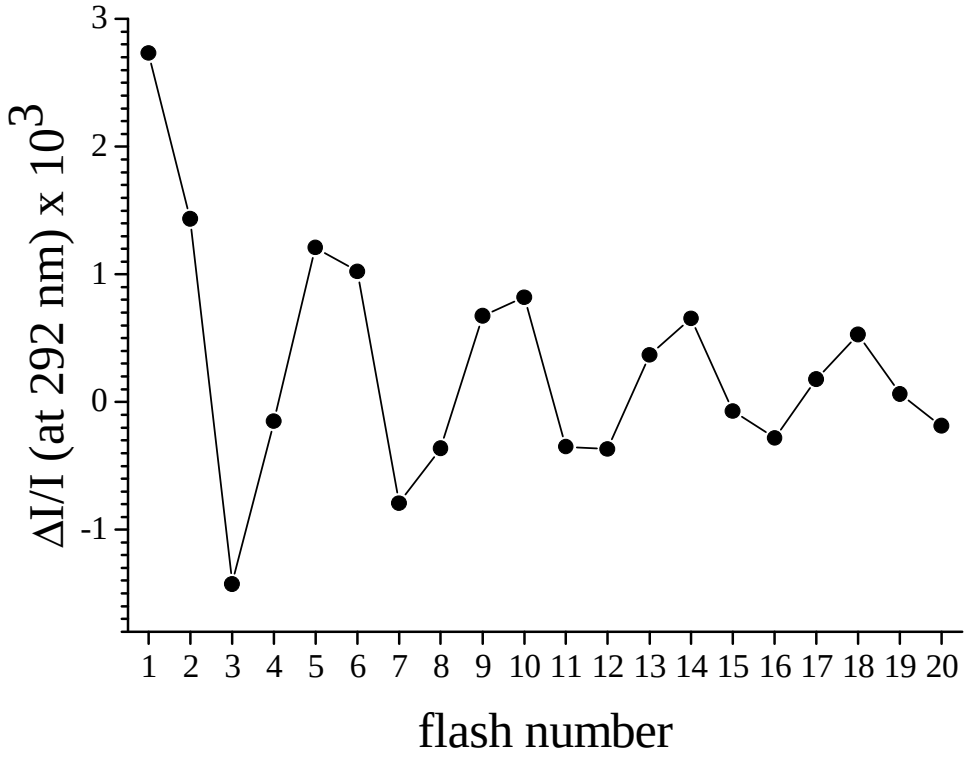
3
2
1
0
-1
ΔI/I (at 292 nm) x 10^3
1 2 3 4 5 6 7 8 9 10 11 12 13 14 15 16 17 18 19 20
flash number

Figure 1

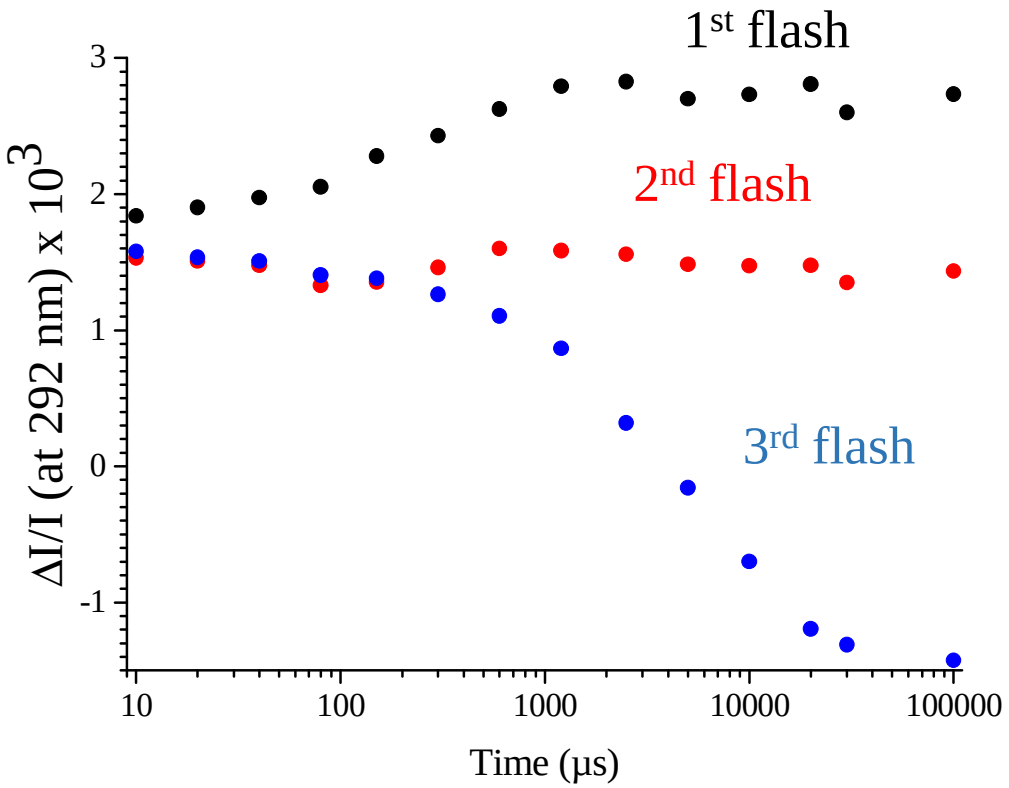
1st flash
2nd flash
3rd flash
ΔI/I (at 292 nm) x 10^3
3
2
1
0
-1
10
100
1000
10000
100000
Time (μs)

Figure 2

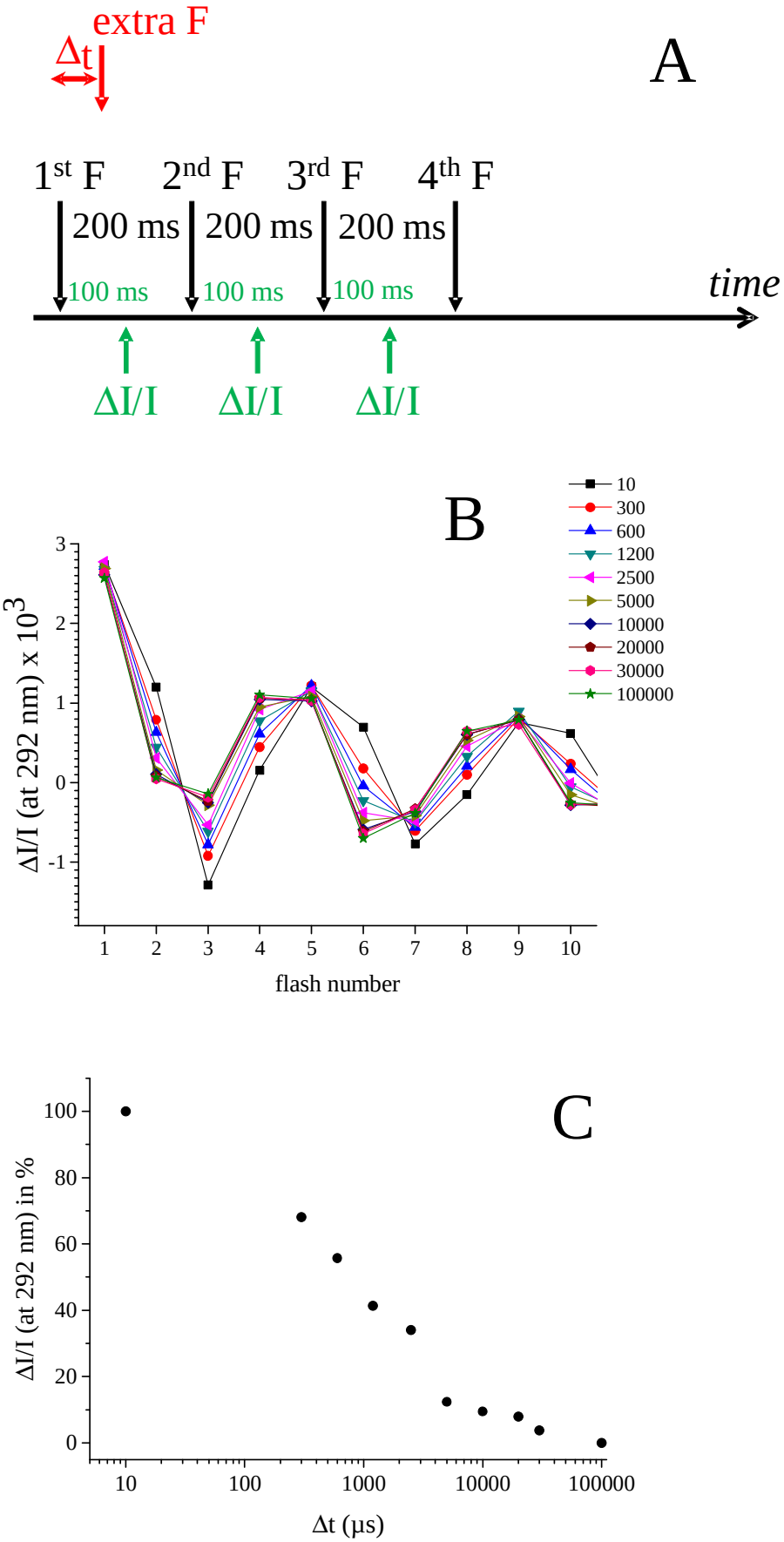
extra F
Δt
A
1st F
2nd F
3rd F
4th F
200 ms
200 ms
200 ms
100 ms
100 ms
100 ms
time
ΔI/I
ΔI/I
ΔI/I
B
10
300
600
1200
2500
5000
10000
20000
30000
100000
ΔI/I (at 292 nm) x 10^3
flash number
C
ΔI/I (at 292 nm) in %
Δt (µs)

Figure 3

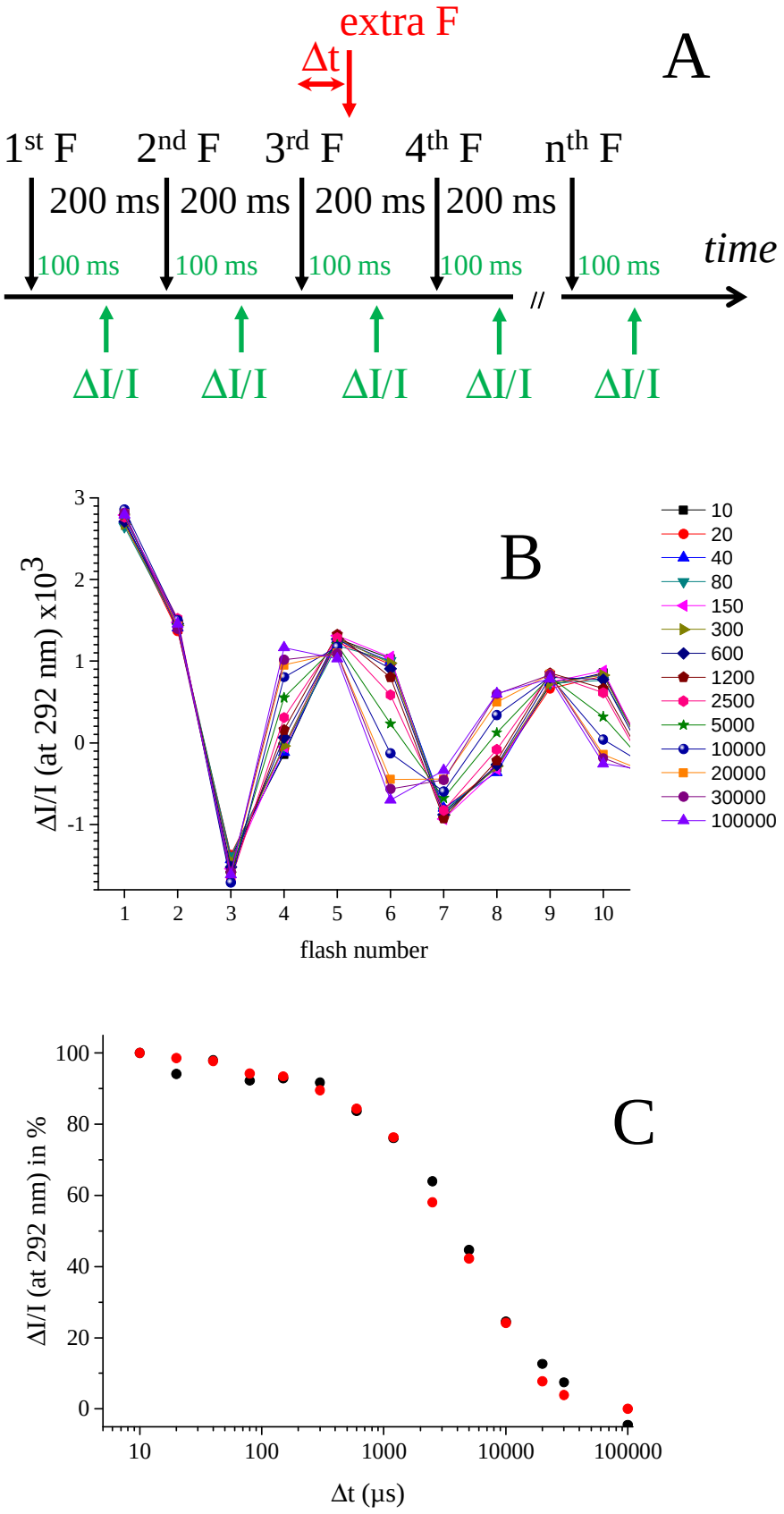
extra F
Δt
A
1st F
2nd F
3rd F
4th F
nth F
200 ms
200 ms
200 ms
200 ms
100 ms
100 ms
100 ms
100 ms
100 ms
time
//
ΔI/I
ΔI/I
ΔI/I
ΔI/I
ΔI/I
B
ΔI/I (at 292 nm) x10^3
flash number
10
20
40
80
150
300
600
1200
2500
5000
10000
20000
30000
100000
C
ΔI/I (at 292 nm) in %
Δt (µs)

Figure 4